China Instrument and Control Society
Instrumentation
INSTRUMENTATION, Vol. 11, No. 1, March 2024 https://doi.org/10.15878/j.instr.202300151

Article

Research on Rotating Machinery Fault Diagnosis Based on Improved Multi-target Domain Adversarial Network

Haitao Wang* **and Xiang Liu**

School of Mechanical and Electrical Engineering, Xi'an University of Architecture and Technology, Xi'an 710055, China

* Corresponding author email: wanghaitao@xauat.edu.cn

Abstract: Aiming at the problems of low efficiency, poor anti-noise and robustness of transfer learning model in intelligent fault diagnosis of rotating machinery, a new method of intelligent fault diagnosis of rotating machinery based on single source and multi-target domain adversarial network model (WDMACN) and Gram Angle Product field (GAPF) was proposed. Firstly, the original one-dimensional vibration signal is preprocessed using GAPF to generate the image data including all time series. Secondly, the residual network is used to extract data features, and the features of the target domain without labels are pseudo-labeled, and the transferable features among the feature extractors are shared through the depth parameter, and the feature extractors of the multi-target domain are updated anatomically to generate the features that the discriminator cannot distinguish. The model t through adversarial domain adaptation, thus achieving fault classification. Finally, a large number of validations were carried out on the bearing data set of Case Western Reserve University (CWRU) and the gear data. The results show that the proposed method can greatly improve the diagnostic efficiency of the model, and has good noise resistance and generalization.

Keywords: multi-target domain; domain-adversarial neural networks; transfer learning; rotating machinery; fault diagnosis

Citation: Haitao Wang and Xiang Liu. "Research on Rotating Machinery Fault Diagnosis Based on Improved Multi-Target Domain Adversarial Network." *Instrumentation* 11, no. 1 (March 2024). https://doi.org/10.15878/j.instr.202300151.

0 Introduction

Rotating machinery, such as bearings and gears, serves as crucial components in transmission systems and finds extensive applications in industries related to national defense security and the national economy, including aerospace and manufacturing.[1] Diagnosis the faults of rotating machinery is beneficial in maintaining the reliability of the machine, reducing the maintenance cost and saving the engineering time. Therefore, timely and accurately identify the type of rotating machinery failure has important research value in practical engineering.[2]

Deep learning theory with the ability of automatically extracting significant features has begun to be applied to end-to-end mechanical intelligent fault diagnosis, and has been widely concerned by scholars at home and abroad[3]. Wang[4] combined Convolutional neural network(CNN) with extrusion excitation network to construct an excitation convolutional neural network (SE-CNN) to achieve bearing fault diagnosis and visualize the realistic bearing state with symmetric point map. Zhao[5] used an asymmetric self-encoder to extract features directly from vibration signals and implemented fault feature information extraction through mapping relationships.

However, the application of intelligent diagnosis methods relies on two critical prerequisites: having sufficient labeled data and consistent data distribution.[6] Since machinery and equipment are mostly operated under different loads and speeds, the measured data often do not obey the same distribution, which leads to a significant degradation of the performance of diagnosis of models learnt from the training set when applied to real-world scenarios. To address the problems with deep learning, Transfer Learning (TL) uses unlabeled target

domain datasets to provide a viable approach to fault diagnosis. Through reducing the difference in distribution between the two domains, TL can share the knowledge gained from the labelled source domain dataset to or from the unlabeled target domain dataset.[7]

Unsupervised Domain Adaptation (UDA) is an important migration learning method, which improves an important idea for solving the fault diagnosis problems in real engineering, and UDA in the existing research contains two major categories, namely, difference-based and adversarial-based domain adaptation.[8] The disparity-based model works by embedding KL divergence and maximum mean difference (MMD) isometric measurements into the adaptive layer of the depth mode. Adversarial-based models enable cross-domain diagnosis by making the source and target domains indistinguishable through adversarial training of feature extractors and domain discriminators.[9] In Recent years scholars have investigated fault diagnosis methods that combine distance measurements and adversarial training in cross domain task. Ding[10] proposed a new depth-domain imbalance adaptive framework that achieves fine-grained latent space matching through classification alignment, introduces margin loss regularization to optimize the classification boundaries of the imbalance fault diagnosis task, and improves the spanning generalization capability. Sun[11] proposed a dynamic multiscale mechanism using Wasserstein distance to build a transfer learning model to solve the problem of diagnostic accuracy reduction caused by feature deviation under different working conditions in fault diagnosis. Zhong[12] combined deep convolutional generative adversarial networks with self-attentive modules and spectral normalization and fine-tuned migration learning for fault diagnosis. Chi[13] by adding soft threshold shrinkage residual network build depth, add the regularization improve alignment between class performance. Qin[14] introduced a wide residual kernel structure to adaptively and adequately extract feature information by dynamically weighting the convolution kernel through the network to achieve effective recognition of bearing faults.

Although scholars have achieved some results in UDA-based fault diagnosis, they have only considered the migration transfer of a single target domain, as shown in Fig.1, which requires re-training the model if the target domain changes, which wastes a lot of time in real scenarios. However, if multiple target domains are simply merged into one target domain, the accuracy rate will be drastically reduced because data from multiple target domains usually do not have the condition of data homogeneous distribution. This paper builds on the work of Mohamed[15] and others to address the more practical UDA problem. As shown in Fig.2, firstly, data preprocessing is carried out using Gram's Corner field to ensure the integrity of fault information. Secondly, set up a multi-target domain migration. Suppose the machine can operate under four different loads 0, 1, 2, 3. When the machine works under load 0, some data has been collected to train the fault diagnosis model. This paper first trains the source feature extractor, using labelled source domains to train the domain discriminator parameters. Then, using the weights of the source domain feature extractor, the target feature extractor weights are initialized to achieve fault classification. Finally, the domain discriminator network is trained to distinguish source domain features from target domain features. To obtain domain invariant features across targets, we adversarial update multiple target domain feature extractors by maximining the domain spacing to generate indistinguishable features for the discriminator. Based on the above critical review, this paper develops a novel framework for rotating machinery diagnosis by integrating DANN and ResNet. Bearings and gears are studied for experimental verification, we work under the assumptions that there are enough labeled samples in the source domain to train the classifier model effectively, that the feature space and label space are the same between the source and multi-target domains, and that the data distributions are different. The main points of the article are as follows:

1) We propose an adversarial multi-target UDA method that design a single-source-domain and multi-target-domain adversarial network model (WDMACN) for solving problems in bearings and gears. The proposed model use Wasserstein distance to calculate the output loss of the classifier. This model effectively solves the problems of the limited scalability of existing approaches.

2) To make the most of the time domain information of vibration signals, a new image coding method called Gram Angle Product Field (GAPF) is proposed in this paper. Data processing via Gram's Angle Field (GAPF) preserves the integrity of fault information to a great extent.

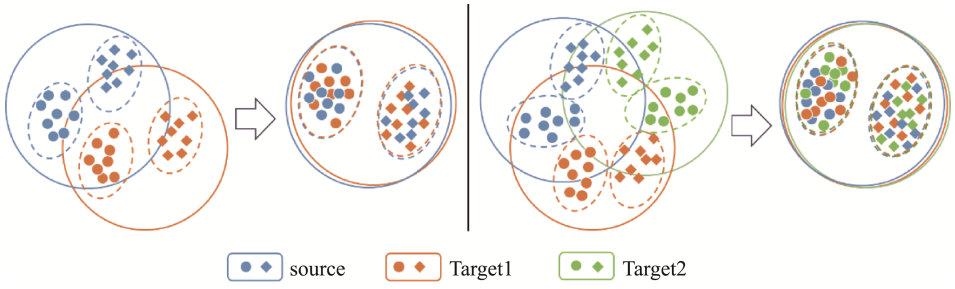

Fig.1 Adaption domain

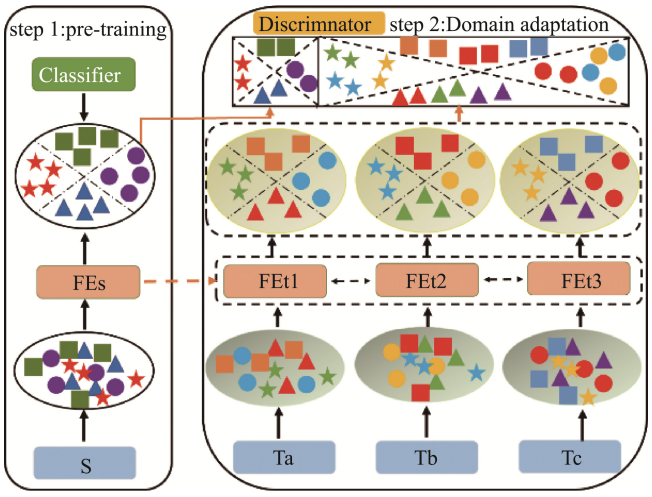

Fig.2 Training process

3) Experiments on bearings and gears is executed for validations. The results show that the proposed model is superior to existing methods.

1 Related Work

Related work for fault diagnosis is briefly introduced, including Gram Angle Product field, domain adversarial networks, deep residual network and Wasserstein distance.

1.1 GAPF

The principle of time domain analysis is simple and easy to implement without loss of information, wavelet analysis and other as common time domain analysis methods can only give the overall effect, not a complete description of the signal instantaneous characteristics. Accordingly, in this paper, the Gram angle product field approach is used for the time domain analysis. The Gram angle product field allows the vibration signal to be converted into image form while preserving the time dependence of the data, ensuring the integrity of the information. The main processes in the Gram's Corner field are as follows[16]:

a. The time series of bearing vibration signals $X=\{x_1, ..., x_i, ..., x_n\}$ is normalized by scaling it through Equation 1 into the interval [–1, 1].

$$\tilde{x}^i = \frac{(x_i - minX) + (x_i - maxX)}{maxX - minX} \tag{1}$$

Where $i = 1, 2, \ldots, n.$.

b. By Equation 2 mapping $\tilde{x}^i$ as an inverse cosine function and time as a radius.

$$\begin{cases} \varphi_i = arccos\left(\tilde{x}^i\right), & -1 \leqslant \tilde{x}^i \leqslant 1,\ \tilde{x}^i \in \tilde{X} \\ r_i = \dfrac{t_i}{N}, & t_i \in N \end{cases} \tag{2}$$

c. Gram's angular difference field and angular sum field matrices are given. Equation 3 is angular difference field and Equation 4 is the angular sum field.

$$G_D = \begin{pmatrix} sin(\varphi_1 - \varphi_1) & \cdots & sin(\varphi_1 - \varphi_n) \\ \vdots & \ddots & \vdots \\ sin(\varphi_n - \varphi_1) & \cdots & sin(\varphi_n - \varphi_n) \end{pmatrix} = \sqrt{I - \tilde{X}'^2} * \tilde{X} - \tilde{X}'^2 * \sqrt{I - \tilde{X}^2} \tag{3}$$

$$G_S = \begin{pmatrix} cos(\varphi_1 + \varphi_1) & \cdots & cos(\varphi_1 + \varphi_n) \\ \vdots & \ddots & \vdots \\ cos(\varphi_n + \varphi_1) & \cdots & cos(\varphi_n + \varphi_n) \end{pmatrix} = \tilde{X}' * \tilde{X}\sqrt{I - \tilde{X}'^2} * \sqrt{I - \tilde{X}^2} \tag{4}$$

where I is the unit row vector. With the above transformations, the time series is transformed into an eigenmatrix, which reflects the relevant information of the vibration signal time series, and is referred to as the Gram matrix.

d. The matrix is converted to a Gram angle product field by using equation (5) to scale each element of the resulting matrix to a size between 0-255, corresponding to the size of each point pixel in the image.

Where $I(j, k)$ denotes the pixel value at the point (j, k) of the image, $int(\cdot)$ is an integer function, and G(j, k) denotes the value of the element corresponding to the jth row and kth column in the matrix.

$$I(j,k) = \text{int}(127.5(\text{G}(\text{j},\text{k}) + 1) \tag{5}$$

e. In order to combine the respective characteristics of the angle difference and sum field, the Gram angle multiplication field GAPF is obtained using equation (6).

$$GAPF = \begin{pmatrix} sin(\varphi_1 - \varphi_1) \times cos(\varphi_1 + \varphi_1) & \cdots & sin(\varphi_1 - \varphi_n) \times cos(\varphi_1 + \varphi_n) \\ \vdots & \ddots & \vdots \\ sin(\varphi_n - \varphi_1) \times cos(\varphi_n + \varphi_1) & \cdots & sin(\varphi_n - \varphi_n) \times cos(\varphi_n + \varphi_n) \end{pmatrix} \tag{6}$$

1.2 Domain Adversarial Neural Networks

The core problem of transfer learning is to reflection source and target domains to a common space and to align distributions within that room. Ganin[17] proposed Domain adversarial neural networks (DANN), DANN draws on the idea of generative adversarial networks. Through adversarial training, the source domain and the target domain are aligned in the feature space, so that the domain discriminator cannot recognize which domain the feature comes from.

Label classifiers are used to output predicted labels. DANN loss function is as follows:

$$l(\theta f,\ \theta y,\ \theta d)=\frac{1}{n_s}\sum_{x_t^s\in \mathrm{D}_s} L_y\left(G_y\left(G_f\left(x_i^s\right)\right),\ y_i^s\right)-\frac{\lambda_D}{n}\sum_{x_m^D\in\left(D_s\cup D_t\right)} L_d\left(G_d\left(G_f\left(x_m^D\right)\right),\ d_m\right) \tag{7}$$

Where: x_m^D is the mth sample in the concatenation of source and target domain samples, n is total number of source domain and target domain samples, and d_m is the domain label. θ_f, θ_y and θ_d are the optimization parameters for G_f, G_y and G_d, respectively, L_y and L_d denote the classifier loss and the discriminator loss function, and λ_D is the weight parameter. The domain adversarial network is trained by max-min optimization as follows:

$$\max_{\theta_d}\ \min_{\theta_f,\theta_y} l(\theta f,\theta y,\theta d) \tag{8}$$

The training enables the feature extractor to eliminate data distribution differences and extract domain invariant features, so that the source domain training classifier can be used directly to the target domain classification to achieve migration diagnosis.

1.3 Deep Residual Network

Convolutional neural network (CNN) has gained strong performance in real-world scenarios, but CNN often has problems with disappearing gradients and explosions as the number of layers deepens. He[18] proposed a deep residual network (ResNet) to solve this problem well, ResNet consists of several residual blocks and its structure is shown in Fig.4.

In the convolutional layer, the convolutional kernel extracts feature in the input mapping with the following operational formula:

$$\mathrm{C}_l=f\left(Ax_l+B\right) \tag{9}$$

Where: x_l and C_l are the input and output mappings in layer l respectively, A is the weight, B is the bias. $f(\cdot)$ is convolution operation.

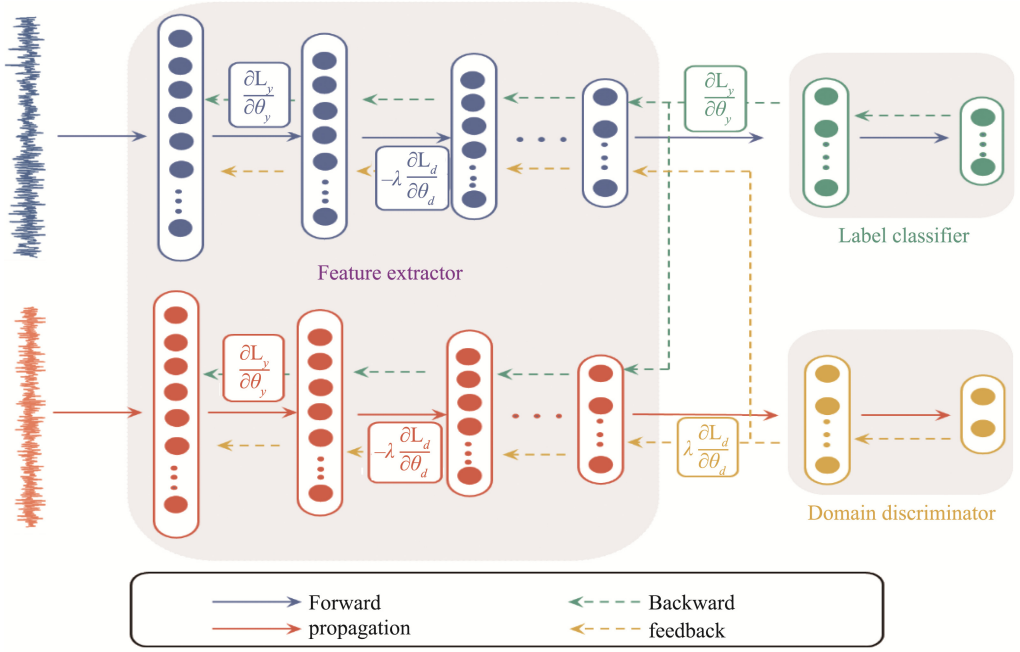

Fig.3 DANN

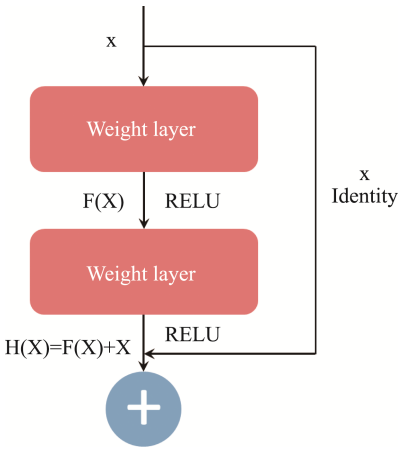

Fig.4 ResNet

The activation function is the RELU function with the operational formula:

$$\varphi(\mathrm{C}_{\ln})=\max(C_{\ln},0) \tag{10}$$

The BN layer can effectively mitigate the gradient disappearance during the training process, and the mean and variance of the data are obtained through the BN layer with the following mathematical formula:

$$\mu_{\mathrm{D}}=\frac{1}{n}\sum_{i=1}^{n}x_i \tag{11}$$

$$\mu_{\mathrm{D}}^2=\frac{1}{n}\sum_{i=1}^{n}(x_i-\mu_D)^2 \tag{12}$$

$$\hat{x}_i=\frac{x_i-\mu_D}{\sqrt{\mu_D^2+\varepsilon}} \tag{13}$$

$$y_i=\gamma\hat{x}_i+\beta \tag{14}$$

Where: x_i and y_i are inputs and outputs, γ and β are learning parameters.

According to the above equation, Residual blocks can be described as follows:

$$\mathrm{Y}=\mathrm{F}(\mathrm{X},\mathrm{W})+X \tag{15}$$

Where: X and Y denote the input and output residual blocks respectively, F(·) mapping operation of the residual block, including convolutional layer, BN layer, RELU function, and W is weight parameter.

1.4 Wasserstein Distance

Wasserstein[19] distance is a valid measure of distance. which is used as a distributional measure function in the domain classifier D to reduce the problem of vanishing gradients, let $p\in[1,\infty)$, for any two probability measures P and Q on M. The formula is described as follows:

$$W_P(P,Q)=\left(\inf_{\pi\epsilon\Pi(P,Q)}E_{(x,y)\sim\pi}[\|x-y\|]\right) \tag{16}$$

Where: $\pi(x, y)$ is the migration strategy from position x to position y, $\rho(x, y)$ is the distance function, and x and y are samples from the set M. $\Pi(P, Q)$ is the set of all P and Q probability measures including the bounds of P and Q. $W_p(P, Q)$ denotes the minimum transport cost under the optimal planning path. Thus the improved function is expressed as follows:

$$\min_{G}\max_{\mathbb{R}}E_{x\sim p}\left[f(x)\right]-E_{x\sim Q}\left[f(y)\right] \tag{17}$$

where $\mathbb{R}$ denotes the set of 1-Lipschitz functions.

DANN in the source and target domain feature extraction process, feature extraction is using convolutional neural network CNN, with the deepening of the number of layers of the network, the network will appear overfitting problem thus leading to not be able to extract the features well. Therefore in this paper we use residual structure for feature extraction and also use Wasserstein difference for learning task specific decision boundaries of the classifier.

2 The Proposed WDMACN Method

This section details the proposed multi-target domain adversarial network model, and our proposed method consists of 2 main steps: (1) Supervised learning on labelled source domains to train the source domain feature extractor E_S; (2) Adversarial training on single source and multi-target domains. The aim of this article is to build a network model in which some shared potential features can be found between source domain and target domains, thus minimaxing the differences between source domain and target domains. The single source multi-target domain proposed in this article is defined as follows:

(1) source domain $D_s=\left\{x_s^i,y_s^i\right\}_{i=1}^{n_s}$, target domain $\{D_{t(1)},\ \ldots,\ D_{t(N)}\}$, $D_{t(j)}=\left\{x_{t(j)}^i\right\}_{i=1}^{n_t}$. Where n_s is the number of samples, $x_s\in X_s$ is the data samples, $y_s^i\in Y_s$ is the corresponding label, N is the number of target domains, $D_{t(j)}$ is all the samples in domain j, $x_{t(j)}^i\in X_{t(j)}$ is the ith sample in domain j, $X_{t(j)}$ is a spatial feature, n_t is the number of unlabeled samples from the target domain.

(2) The feature spaces of the source and target domains have the same label space and different edge distributions:

$X_s=X_{t(1)}=\ldots X_{t(N)}$, $Y_s=Y_{t(1)}=\ldots=Y_{t(N)}$, $P_s(X)\neq P_{t(j)}(x)$, $P_{t(j)}(x)\neq P_{t(i)}(x)$, where N is a sample of the target domain, $j\neq i$.

2.1 Model Structure

Fig.5 shows the model proposed in this paper. The WDMACN model consists of three parts: feature extractor, label classifier and domain discriminator. The feature extractor E consists of a residual block and a maximum pooling layer, and the source domain feature extractor Es and the target domain feature extractor E_t with bound weights are constructed through E. The label classifier C is used to predict the classification labels for the source domain and target domains, and the domain discriminator D is used to distinguish from which domain the data samples is come.

1) Feature extractor: train the labelled source domain $D_s=\left\{x_s^i,y_s^i\right\}_{i=1}^{n_s}$, save the parameters of the feature extractor Es, and extract features from N target domains at the same time, and bind the weights to all the target feature extractors to find a new common feature, so that the common weights of the target extractors can reflect any target domain. To better illustrate the model proposed in this paper, the parameters θ_h and G_h are used to denote the feature extractor function. The inputs x_s^i and $x_{t(j)}^i$, which have been processed by the Gram's corner field, are mapped by the feature extractor into multidimensional feature vectors $h_s^i=G_h\left(x_s^i;\theta_h\right)$ and $h_{t(j)}^i=G_h(x_{t(j)}^i;\theta_h)$, where h_s^i denotes the output of the ith sample and $h_{t(j)}^i$ denotes the output of the ith sample in the jth target domain. Deep features are represented by $H_s=G_h\left(x_s;\theta_h\right)$ and $H_{t(j)}=G_h\left(x_{t(j)};\theta_h\right)$.

2) Label classifiers: a labelled classifier is trained using a labelled source domain, and the classifier C is supervised by minimaxing the loss of cross-entropy between predicted and true labels, denoted by the parameters θ_c and G_c for the classifier function.

$$L_c\left(x_s^i,y_s^i\right)=-\frac{1}{n^s}\left[\sum_{i=1}^{n^s}\sum_{m=1}^{M}l\left(y_s^i=m\right)\log\left(G_c\left(G_h\left(x_s^i;\theta_h\right);\theta_c\right)\right)_m\right] \tag{18}$$

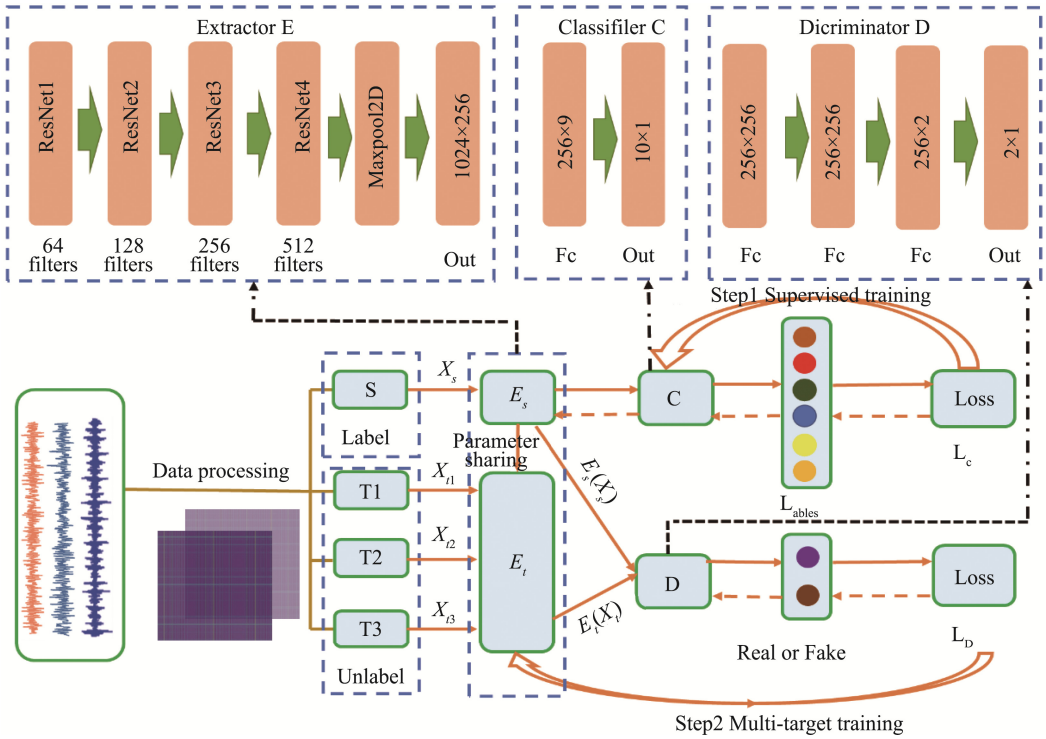

Fig.5 Single-source multi-target domain WDMACN fault diagnosis model

3) Domain discriminator: the deep features H_s and $H_t(j)$ are fed into a domain classifier with parameters θ_w and G_w . The Wasserstein distance formula between H_s and $H_t(j)$ is defined as follows: G_w meet the 1-Lipschitz function constraint, and add a gradient penalty term that reduces to

$$W_P\left(P_{H_s};P_{H_{t(j)}}\right)=\sup_{\|G_w\|_L\leqslant 1}E_{P_{H_s}}\left[G_w\left(G_h\left(x_s;\theta_h\right);\theta_w\right)\right]-E_{P_{H_{t(j)}}}\left[G_h\left(x_{t(j)};\theta_h\right);\theta w\right] \tag{19}$$

$$L_{w(j)}\left(x_s^i,x_{t(j)}\right)=\frac{1}{n_s}\sum_{x_s\in Ds}G_w\left(G_h\left(x_s;\theta_h\right);\theta_w\right)-\frac{1}{n_{t(j)}}\sum_{x_{t(j)}\in D_{t(j)}}G_w\left(G_h\left(x_{t(j)};\theta_h\right);\theta_w\right)-\alpha\left(\left\|\nabla_{\hat{H}}G_w\left(\hat{H};\theta_w\right)\right\|_2-1\right)^2 \tag{20}$$

Where: $L_{w(j)}\left(x_s^i,x_{t(j)}\right)$ is the domain classifier loss of the source domain with respect to the jth target domain, $\hat{H}$ denotes uniform sampling, and α is the compromise parameter. Calculate the Wasserstein distance by maximizing the loss function.

$$L_D=\frac{1}{N}\left(\beta_0L_{w(1)}+\cdots+\beta_{N-1}L_{w(N)}\right) \tag{21}$$

Where: $\beta_0\cdots\beta_{N-1}$ is the compromise parameter

2.2 Model Training

The parameter θ_w is adjusted to maximize the domain discriminator loss function, the feature extractor parameter θ_h is adjusted to minimize the Wasserstein distance. The objective of the optimization function of the domain discriminator is describe as:

$$\theta_w=\arg\max_{\theta_w}L_D \tag{22}$$

$$\theta_h=arg\min_{\theta_h}L_D \tag{23}$$

Combining the label classification loss with the domain discriminator loss yields the total loss function:

$$L_{total}=L_C+\gamma L_D \tag{24}$$

Where: γ is the compromise parameter.

The training process is shown in Fig.2, firstly supervised training of the source domain, training the parameters θ_h and θ_c, by Equation 24; secondly, unsupervised adversarial training of the multi-objective domain, calculating the loss function by Equation 20, updating the parameters θ_h and θ_w by using Equation 22 and 23, and updating the weight parameters by using the SGD stochastic algorithm during the training process.

3 Experimental Verification

In order to verify the superiority of the proposed model WDMACN, thesis is validated on the gear dataset measured at the experimental bench and the Case Western Reserve University bearing dataset. The hardware and software information used in this experiment is as follows: 64-bit Windows 10 operating

system is used, GPU is NVIDIA GTX3070 and CPU is Intel i5. The procedure uses the SGD optimizer to update the network and during training, the number of iterations, the number of pips, and the SGD learning rate of the deep learning model are set to 50, 32, and 0.0001, respectively. The training and validation sets of the experimental data are randomly divided according to a 7:3 ratio. To prevent overfitting of the model, we set the dropout value of the dropout layer to 0.5. Fault types are categorized using the Softmax classification function.

3.1 Gearbox Experiments

3.1.1 Gearbox Experiment Data Set

To verify the feasibility of the model in real working conditions, the planetary gearbox data are collected. Experimental platform for data acquisition of gear box is shown in Fig.6, which consists of an electric motor, a fixed-shaft gearbox, and a planetary gearbox. Using this experimental platform, vibration signals can be obtained from 7 measurement points, 5 speeds for specific loads, each load containing three types of faults: normal faults, broken tooth faults, and cracked tooth faults. In this paper, the vibration signals are selected for measurement point 1 position, 1260, 1500, 900, and 1470 r/min conditions. A total of 3 different categories of faults are obtained, and 2000 samples are collected for each fault, each consisting of 1024 data points. The experimental data set is shown in Table 1. One display is taken for each data type as shown in Fig.7.

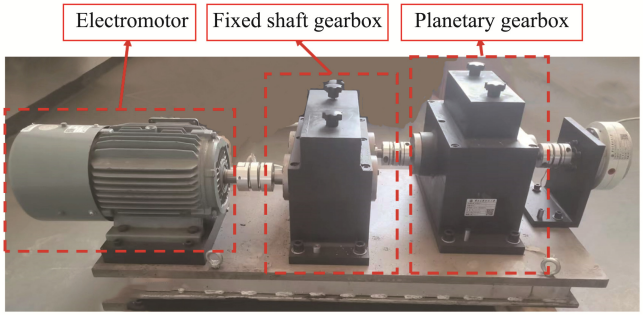

Fig.6 Gearbox experimental platform

Table 1 Gearbox data description

Condition	Fault type	Normal	Tooth broken	Tooth fracture	Motor speed/r.min^{-1}
A	Training sample	1400	1400	1400	1260
	Test sample	600	600	600	
B	Training sample	1400	1400	1400	1500
	Test sample	600	600	600	
C	Training sample	1400	1400	1400	900
	Test sample	600	600	600	
D	Training sample	1400	1400	1400	1470
	Test sample	600	600	600	

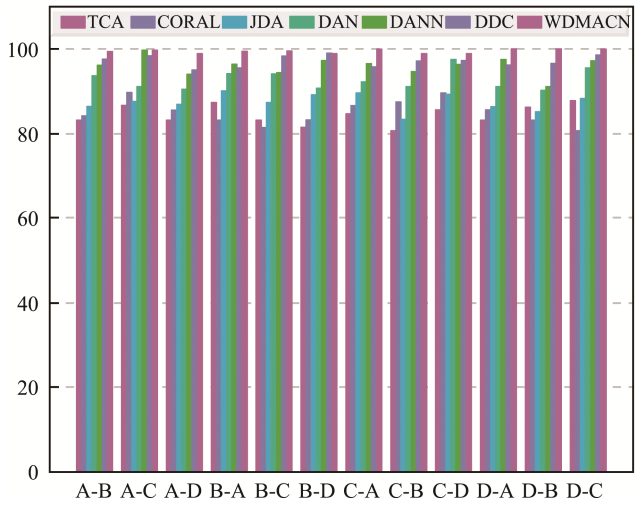

Fig.7 Gearbox accuracy rate

3.1.2 Discussion and Analysis of Experimental Results

In order to evaluate the performance of the proposed model WDMACN model, 12 cross-domain experiments are conducted in this paper, and the results are compared with six different methods, including the results TCA[20],CORAL[21],JDA[22] DAN[23],DANN[17] and DDC[24]. As shown in Table 2, a bar chart of Table 2 is given in Fig.8 for a clearer comparison of the obtained results with other methods. In the first three experiments (A-B, A-C, A-D), we used dataset A as the source domain and B, C, and D as multiple target domains to learn feature extractors, classifiers, and discriminators, and then each individual target domain B, C, and D was tested on the learnt feature extractors to generate A-B, A-C, and A-D migrations, and similarly we used B, C, and D as the source domains for the cross-domain experiments. Table 2 evaluates the 12 different migration methods, and among the 12 cross-domain migrations, 10 cross-domain migrations outperform the other models, and WDMACN achieves an average accuracy of 99.48%, which is an improvement of 2.33% compared to DDC. This indicates that the model proposed in this paper is able to better achieve migration learning at different speeds. Since the depth model has an uninterpretable under in the feature extraction stage, in order to verify the effect of WDMACN one by one, the t-SNE algorithm is used to visualize the output results of the network's input layer, residual block 1, residual block 3 and output layer. Fig.8 gives the visualization results for each layer under the A-B migration task. As shown in Fig.9,

Table 2 Accuracy rate of gearbox

Method	TCA	CORAL	JDA	DAN	DANN	DDC	WDMACN
A-B	83.26%	84.21%	86.44%	93.71%	96.16%	97.62%	99.41%
A-C	86.71%	89.74%	87.63%	91.11%	99.73%	98.42%	99.7%
A-D	83.24%	85.61%	86.97%	90.54%	94.05%	95.04%	98.92%
B-A	87.43%	83.22%	90.12%	94.21%	96.42%	95.56%	99.48%
B-C	83.2%	81.47%	87.43%	94.13%	94.43%	98.33%	99.51%
B-D	81.54%	83.32%	89.21%	90.73%	97.31%	99.06%	98.93%
C-A	84.73%	86.63%	89.66%	92.28%	96.52%	95.83%	99.96%
C-B	80.77%	87.54%	83.41%	91.15%	94.71%	97.17%	98.92%
C-D	85.64%	89.61%	89.31%	97.51%	96.34%	97.29%	98.93%
D-A	83.21%	85.64%	86.43%	91.14%	97.51%	96.24%	100%
D-B	86.31%	83.21%	85.23%	90.27%	91.14%	96.62%	100%
D-C	87.83%	80.72%	88.72%	95.53%	97.21%	98.62%	99.98%

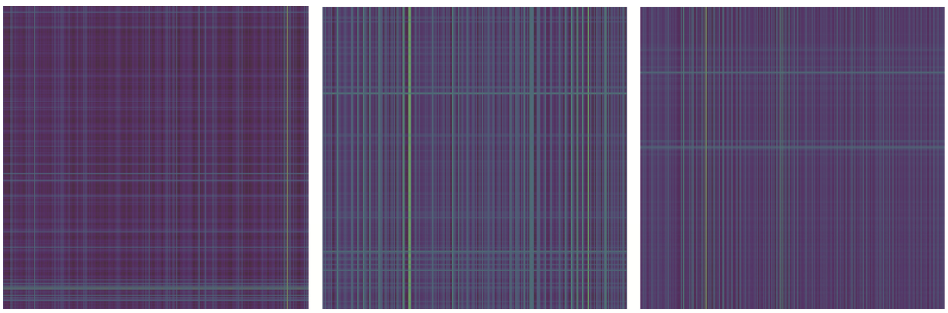

a. Normal b. Tooth broken c. Tooth fracture

Fig.8 GAPF feature maps with different data labels

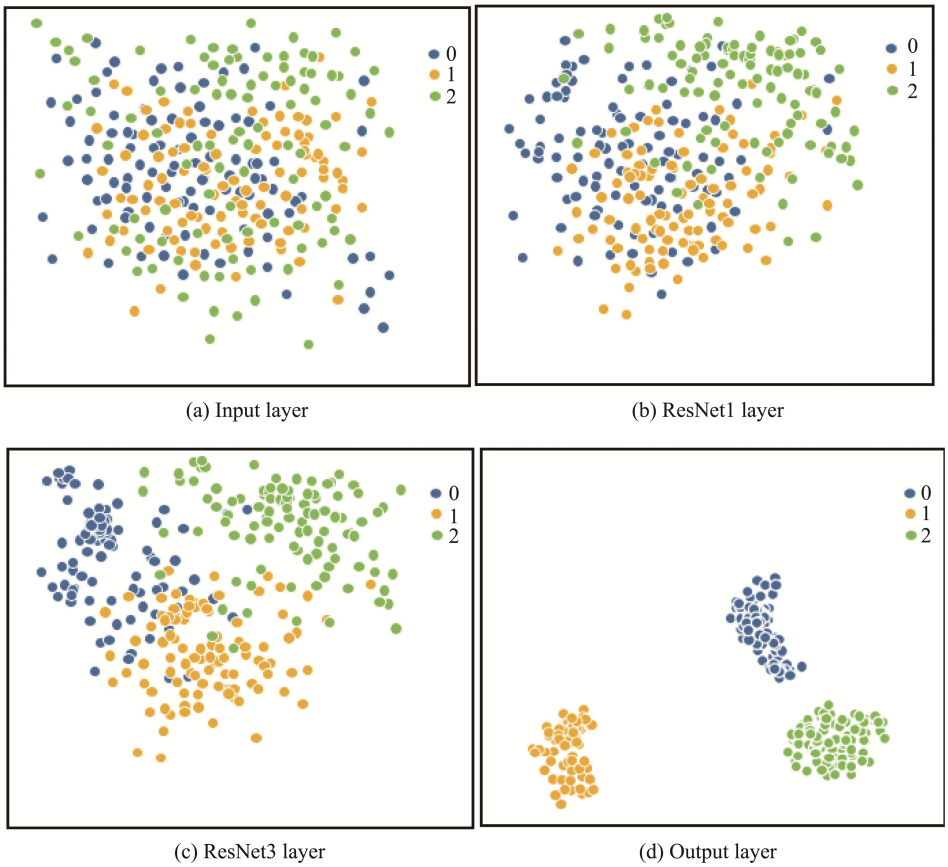

(a) Input layer (b) ResNet1 layer

(c) ResNet3 layer (d) Output layer

Fig.9 Visualization of WDMACN model in gearbox dataset

when the image first enters the network, the distribution of the three fault types is confusing because the features have not yet been extracted, and the various fault types cannot be clustered, and when the network reaches the residual block 3, the network learns some fault information and can be roughly clustered, but there is still confusion at the fault boundaries. By the time the fault reaches the output layer, the network has sufficiently learnt the fault features and the fault classification is significantly improved.

3.1.3 Experimental Analysis of Fault Diagnosis Under Noise Interference

In real scenarios, the acquired vibration signals are susceptible to external interference, and in order to verify the immunity of WDMACN in noise, Gaussian white noise with different signal-to-noise ratios (SNR) is added to the original signals, and the SNR is defined as follows:

$$SNR(dB)=10\log_{10}\left(\frac{P_{signal}}{P_{noise}}\right) \tag{25}$$

To verify the robustness of WDMACN under noise. Gaussian white noise of 0, –3dB and –6dB is added to the acquired vibration signals, respectively, and the model accuracies under different noise disturbances are shown in Fig.10 in the migration task of A-B. From the table, it can be seen that the fault identification accuracy of various networks decreases gradually with the decreasing signal-to-noise ratio. The decreases of the seven models with added noise are 12.26 %, 15.1 %, 15.83 %, 17.17 %, 13.85 %, 9.51 %, and 5.45 %, respectively. The accuracies of WDMACN are all higher than the other models in the noiseless condition and the decrease is smaller. Therefore, the WDMACN model is more stable and has better resistance to noise interference and robustness.

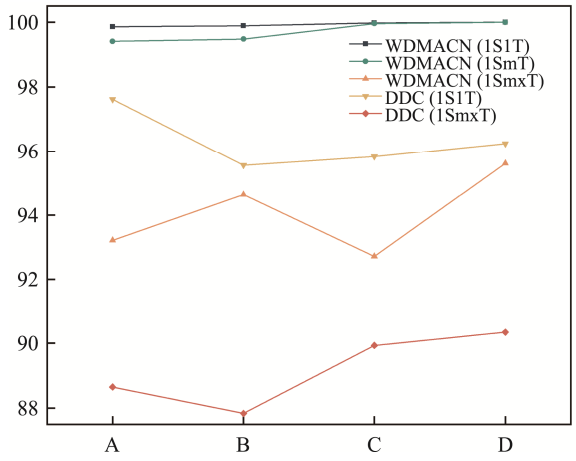

Fig.10 Accuracy of each model under different noise

3.1.4 Single Source Domain Multi-target Domain Efficiency Validation

In this section, a comparison is made in terms of model generalizability and time efficiency by setting up a single-source single-target domain (1S1T) and a unitary multi-target domain (1SmT). For single-source single-target domains, this paper adopts the DDC method for comparison, in addition to single-source single-target domains and single-source multi-target domains, this paper also constructs a single-source mixed-target domain (1SmxT) by mixing N target domains into a single target domain, and the results are shown in Fig.11.

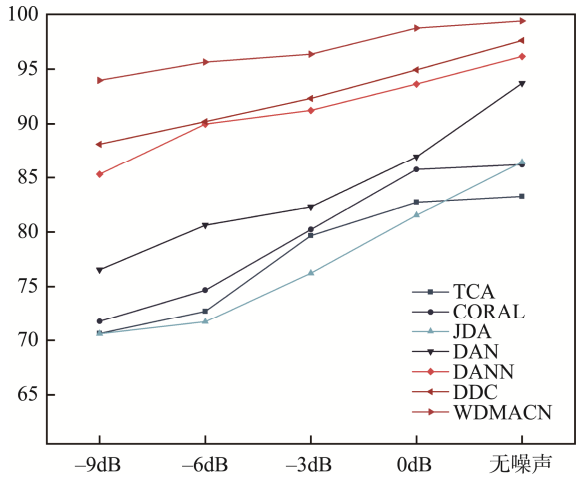

Fig.11 Accuracy of different target domain Settings

Where 1S1T and 1SmT are tested with B as the target domain when A is the source domain, and all are tested with A as the target domain when B, C and D are the source domain. From the table, it can be seen that the accuracy of the proposed model WDMACN (1SmT) is improved by 5.65% compared to WDMACN (1SmxT), which is also significantly better than DDC. In addition, to verify the efficiency of the model, the training times for 1S1T and 1SmT were compared as shown in Table 3, which shows the training times for the A condition migrated to the B, C, D unit single target and unit multi-target settings. From the table, it can be seen that the training time of the proposed model is much less than the training time of the single target domain, which indicates that our proposed model can significantly reduce the training time. Therefore, the WDMACN (1SmT) proposed in this paper is more suitable for real industrial scenarios.

Table 3 Training time of single target domain and multi-target domain

Model	Training time /s
1S1T	6174.4
1SmT	2573.5

3.1.5 Algorithm Convergence

To prove the convergence of the proposed function, the loss function during migration iterations is recorded. As shown in Fig.12A-B the loss function in the task. From the figure, it can be seen that the training process of the proposed method are convergent and can converge faster compared to other algorithms.

3.2 Case Western Reserve University Rolling Bearing Experiments

3.2.1 Description of the Data Set

To further validate the feasibility of the proposed model in real working conditions, the proposed method was tested using the Case Western Reserve University (CWRU) rolling bearing experimental dataset.[25]

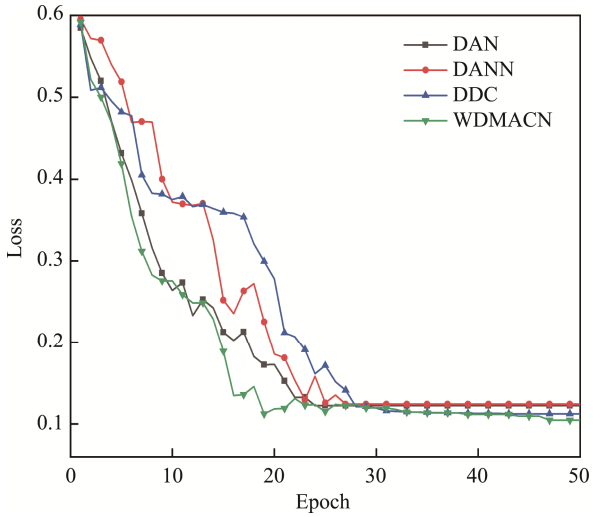

Fig.12 loss curve of fault identification

The experimental platform for data acquisition is shown in Fig.13, which consists of a motor, torque transducer, power test meter, and electronic controller with a sampling frequency of 12 KHz.

Using this experimental platform it is possible to obtain four specific loads of 0, 1, 2 and 3 rotational speeds, and each load contains three types of faults: damage failure of the inner ring, damage failure of the outer ring, and damage failure of the rolling body. In addition, each fault contained three more types of 0.07, 0.14, and 0.21 inches depending on the size of the damage. A total of nine different categories of faults were obtained, and 2000 samples were collected for each fault, each consisting of 1024 data points. The experimental data set is shown in Table 4.

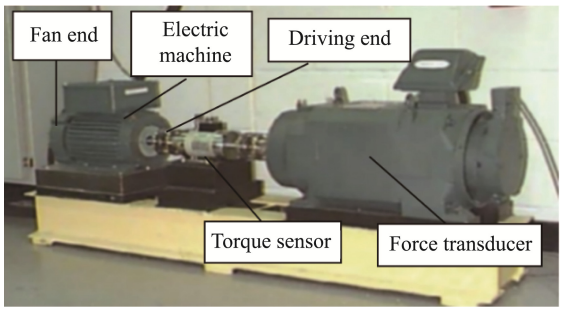

Fig.13 CWRU experimental platform

3.2.2 Discussion and Analysis of Experimental Results

Table 5 shows the results obtained under the gearbox dataset, and to compare the obtained results with other methods more clearly, a bar chart of Table 5 is given in Fig.14. From the table, it can be seen that out of the six cross-domain faults in the diagnosis experiments, five cross-domain migrations outperform the other models, and WDMACN achieves an accuracy of 99.47 per cent, which is an improvement of 1.17 % compared to DDC.

This further indicates that the model proposed in this paper outperforms other models. Similarly, to verify the effect of WDMACN on GAPF feature extraction on a layer-by-layer basis, the t-SNE algorithm was used to visualize the output results of the input layer, residual block 1. residual block 3 and output layer of the network. Fig.15 gives the visualization results for each layer under the E-F migration task.

Table 4 CWRU experimental data set

Condition	Fault type	Ball			Inner			Outer			Motor speed/ r·min^{-1}
	Fault size(inch)	0.07	0.14	0.21	0.07	0.14	0.21	0.07	0.14	0.21	
E	Training sample	1400	1400	1400	1400	1400	1400	1400	1400	1400	1979
	Test sample	600	600	600	600	600	600	600	600	600	
F	Training sample	1400	1400	1400	1400	1400	1400	1400	1400	1400	1772
	Test sample	600	600	600	600	600	600	600	600	600	
G	Training sample	1400	1400	1400	1400	1400	1400	1400	1400	1400	1750
	Test sample	600	600	600	600	600	600	600	600	600	

Table 5 Accuracy rate of CWRU

Method	TCA	CORAL	JDA	DAN	DANN	DDC	WDMACN
E-F	79.32%	81.75%	85.18%	85.83%	94.43%	98.42%	99.25%
E-H	76.63%	78.73%	86.04%	86.11%	98.64%	97.76%	99.42%
F-E	80.78%	83.72%	89.93%	89.73%	94.45%	96.87%	98.61%
F-H	79.93%	81.63%	87.02%	84.03%	98.89%	99.97%	99.91%
H-E	83.73%	79.94%	86.11%	87.09%	97.64%	97.63%	99.91%
H-F	77.62%	82.22%	84.96%	87.12%	96.66%	98.94%	99.67%

Fig.14 CWRU accuracy rate

4 Conclusion

In this paper, a multi-objective domain migration learning model, WDMACN, is proposed to address the problem of degraded fault diagnosis performance of rotating machinery under variable operating conditions. Good diagnostic results are obtained through experimental validation on gearbox dataset and CWRU bearing dataset, and the following conclusions are drawn:

(1) Firstly, the features of multiple target domains are extracted simultaneously using residuals in the feature extraction stage, and a potential space that can represent the features of all target domains is found to represent the new target domain. Secondly, the Wasserstein distance, which measures the distribution metric between two domains, is used in conjunction with the adversarial training method in domain adaptation to ensure the stability of the training process. Finally, extensive experimental validation in CWRU dataset and gearbox dataset and comparison with several mainstream models show that the method proposed in this paper can effectively realize multi-objective domain fault diagnosis.

(2) In this paper, Gaussian white noise of 0dB, -3dB and -6dB is added to the data samples to simulate the ambient noise in the real scene, and more than 98.6% recognition accuracy is obtained in all the CWRU datasets with the A working condition as the source domain, and the accuracy is improved by more than 4.4% compared with the other models, which proves that the proposed model in this paper has a good noise immunity.

(3) Compared with the single-source domain single-target domain model, the multi-source multi-target domain training model can significantly reduce the training time and effectively improve the training efficiency, which will be more relevant in engineering.

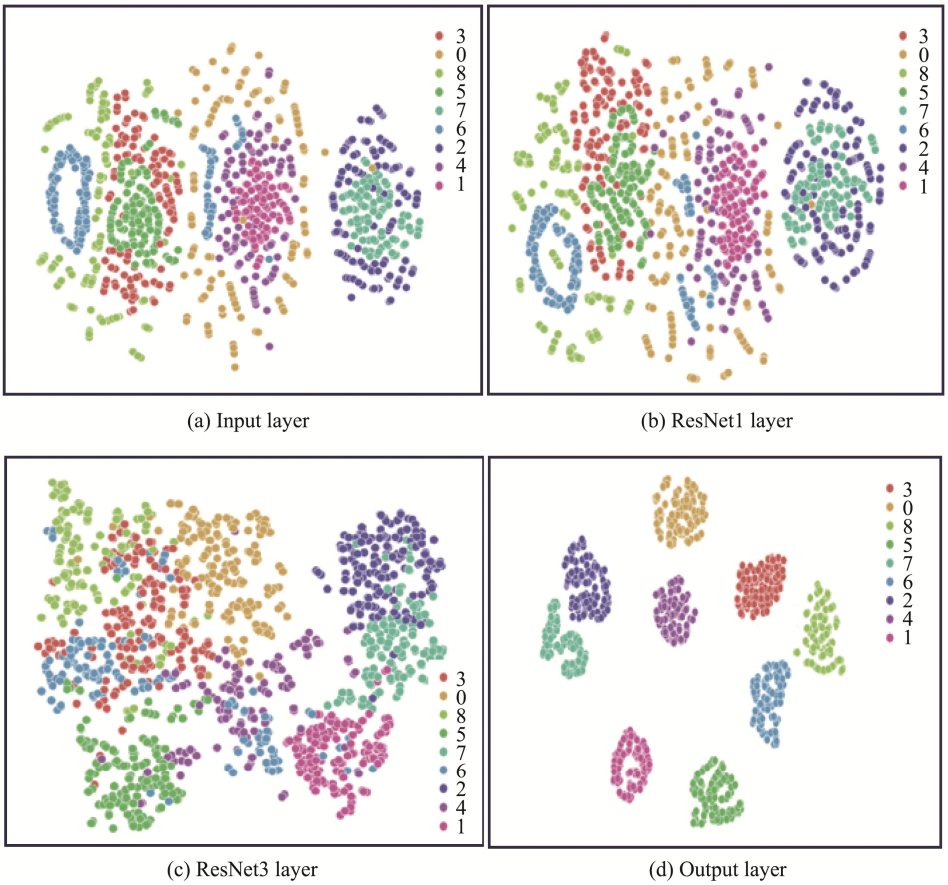

(a) Input layer (b) ResNet1 layer

(c) ResNet3 layer (d) Output layer

Fig.15 Visualization of WDMACN model in rolling bearing data

Author Contributions:

Conceptualization, Wang.Haitao and Liu.Xiang; formal analysis, Wang.Haitao; writing-original draft preparation, Liu.Xiang; writing-review and editing: Liu.Xiang; project administration: Liu.Xiang; funding acquisition: Wang.Haitao.

Funding Information:

Shaanxi Province key Research and Development Plan - Listed project (2022-JBGS-07).

Data Availability:

The data supporting this are from previously reported studies and datasets, which have been cited.

Conflict of Interest:

The authors declare no conflict of interest.

Dates:

Received 20 September 2023; Accepted 28 December 2023; Published online 31 March 2024

References

[1] Li, W, Zhong, X, Shao, H, et al. (2022). Multi-mode data augmentation and fault diagnosis of rotating machinery using modified ACGAN designed with new framework[J]. Advanced Engineering Informatics, 2022,52, Article 101552

[2] Wu, Z., Jiang, H., Zhu, H., et al. (2023a) A knowledge dynamic matching unit-guided multi-source domain adaptation network with attention mechanism for rolling bearing fault diagnosis[J]. Mechanical Systems and Signal Processing, 189, Article 110098.

[3] JIANG Hongkai, SHAO Haidong, LI Xingqiu. Deep learning theory with application in intelligent fault diagnosis of aircraft[J]. Journal of Mechanical Engineering, 2019, 55(7): 27-34.

[4] H. Wang, J. Xu, R. Yan, and R. X. Gao, “A new intelligent bearing fault diagnosis method using SDP representation and SE-CNN,” IEEE Trans. Instrum. Meas., vol. 69, no. 5, pp. 2377-2389, May 2020.

[5] ZHAO Zhihong, LI Lehao, Y ANG Shaopu, et al. A Frequency Domain Feature Extraction Auto-encoder and Its Applications on Fault Diagnosis[J]. China Mechanical Engineering, 2021, 32(20): 2468-2474.

[6] Mohajer, A., Daliri, M. S., Mirzaei, A., et al. (2022a). Heterogeneous computational resource allocation for NOMA: Toward green mobile edge-computing systems[J].

[7] Dong, S., Zhan, J., Hu, W., et al. (2023). Energy-efficient hierarchical resource allocation in uplink-downlink decoupled NOMA HetNets [J]. IEEE Transactions on Network and Service Management. Jinghui Tian, Dongying Han, Mengdi Li, Peiming Shi, A multi-source information transfer learning method with subdomain adaptation for cross-domain fault diagnosis, Knowledge- Based Systems, Volume 243,2022,108466, ISSN 0950-7051

[8] Y. Zhu, F. Zhuang, D. Wang, Aligning domain-specific distribution and classifier for cross-domain classification from multiple sources, in: Proceedings of the AAAI Conference on Artificial Intelligence, 2019, pp. 5989-5996.

[9] B. Yang, S. Xu, Y. Lei, C. Lee, E. Stewart, C. Roberts, Multi-source transfer learning network to complement knowledge for intelligent diagnosis of machines with unseen faults, Mech. Syst. Sig. Process. 162 (2022), 108095.

[10] J. Yosinski, J. Clune, Y. Bengio, H. Lipson, How transferable are features in deep neural networks? in: Adv. Neural Inf. Process. Syst, 2014, pp.3320-3328

[11] Yifei Ding, Minping Jia, Jichao Zhuang, Yudong Cao, Xiaoli Zhao, Chi-Guhn Lee, Deep imbalanced domain adaptation for transfer learning fault diagnosis of bearings under multiple working conditions, Reliability Engineering & System Safety, Volume 230,2023,108890, ISSN 0951-8320, https://doi.org/10.1016/j.ress.2022.108890.

[12] Xinjie Sun, Shubiao Wang, Jiangping Jing, Zhangliang Shen, Liudong Zhang, Fault Diagnosis Using Transfer Learning With Dynamic Multiscale Representation, Cognitive Robotics (2023), doi: https://doi.org/10.1016/ j.cogr.2023. 07.006.

[13] Hongyu Zhong, Samson Yu, Hieu Trinh, Yong Lv, Rui Yuan, Yanan Wang, Fine-tuning transfer learning based on DCGAN integrated with self-attention and spectral normalization for bearing fault diagnosis, Measurement, Volume 210,2023, 112421, ISSN 0263-2241, https://doi.org/ 10.1016/ j.measurement.2022.112421.

[14] CHI Fulin, YANG Xinyu, SHAO Siyu, et al.Bearing fault diagnosis under variable working condition based on deep residual shrinkage networks, Computer Integrated Manufacturing Systems,2023,29(04):1146-1156.

[15] QIN Guohao, ZHANG Kai, DING Kun, HUANG Fengfei1, ZHENG Qing, DING Guofu. Dynamic wide convolutional residual network for bearing fault diagnosis[J/OL]. China Mechanical Engineering: 1-9[2023-08-04]. TH.20230628. 1516.006.html.

[16] RAGAB, MOHAMED, CHEN, ZHENGHUA, WU, MIN, et al. Adversarial Multiple-Target Domain Adaptation for Fault Classification[J]. 2021,703500211-1-3500211-11. DOI:10.1109/

TIM.2020.3009341.

[17] HAITAO WANG , YIFAN GUO , XIANG LIU , JIE YANG , XIHENG ZHANG , AND LICHEN SHI, Fault Diagnosis Method for Imbalanced Data of Rotating Machinery Based on Time Domain Signal Prediction and SC-ResNeSt. Access, VOLUME 11, 2023

[18] GANIN Y, USTINOVA E, AJAKAN H, et al. Domain-adversarial training of neural networks［J］. Journal of Machine Learning Research, 2016, 17(1): 2097

[19] K. He, X. Zhang, S. Ren, J. Sun, Deep residual learning for image recognition, in: 2016IEEE Conference on Computer Vision and Pattern Recognition, 2016, pp. 770-778.

[20] Walczak S. Wasserstein distance. Springer International Publishing; 2017.

[21] S. J. Pan, I. W. Tsang, J. T. Kwok, and Q. Yang, “Domain adaptation via transfer component analysis,” IEEE Trans. Neural Netw., vol. 22,no. 2, pp. 199-210, Feb. 2011.

[22] B. Sun, J. Feng, and K. Saenko, “Correlation alignment for unsuper-vised domain adaptation,” in Domain Adaptation in Computer Vision Applications. Cham, Switzerland: Springer, 2017, pp. 153-171, doi:10.1007/ 978-3-319-58347-1_8.

[23] M. Long, J. Wang, G. Ding, J. Sun, and P. S. Y u, “Transfer feature learning with joint distribution adaptation,” in Proc. IEEE Int. Conf. Com put. Vis., Dec. 2013, pp. 2200-2207.

[24] Y. Song, Y. Li, L. Jia, and M. Qiu, “Retraining strategy-based domain adaption network for intelligent fault diagnosis,” IEEE Trans. Ind. Informat, vol. 16, no. 9, pp. 6163-6171, Sep. 2020.

[25] ZHAO, KE, JIANG, HONGKAI, WANG, KAIBO, et al. Joint distribution adaptation network with adversarial learning for rolling bearing fault diagnosis[J]. Knowledge-based systems, 2021, 222(Jun.21):106974.1-106974.12.

[26] W.A. Smith, R.B. Randall, Rolling element bearing diagnostics using the case western reserve university data: A benchmark study, Mech. Syst. Signal Proces. 64 (2015) 100-131.